RESEARCH ARTICLE

EPAS1 amplifies asthma pathogenesis through JAK2/STAT3-mediated ferroptosis and inflammation

Lili Liu[1], Cheng Yang[2], Yan Li[1], Hao Zhou[1], Mei Shi[1], Tiantian Shi[3], Weibing Shi[1*]

[1]The First Affiliated Hospital of Anhui University of Chinese Medicine, Hefei, Anhui, China;

[2]The Second Affiliated Hospital of Anhui University of Chinese Medicine, Hefei, Anhui, China;

[3]Anhui University of Chinese Medicine, Hefei, Anhui, China.

*Correspondence to **Weibing Shi** : swbsxj@163.com

ABSTRACT

Asthma is a chronic respiratory disorder marked by airway hyperresponsiveness and inflammation, yet the specific molecular mechanisms driving these processes remain only partially understood. This study aims to better understand how the JAK2/STAT3/EPAS1 axis regulates inflammation and ferroptosis in asthma. Asthma-related datasets were retrieved from the Gene Expression Omnibus (GEO) database, and differentially expressed genes (DEGs) were identified. Weighted Gene Co-expression Network Analysis (WGCNA) was used to detect gene modules associated with asthma. A protein-protein interaction (PPI) network was then constructed by intersecting WGCNA-derived genes with ferroptosis-related genes to identify key hub genes. The diagnostic value of these ferroptosis-associated genes was evaluated using Receiver Operating Characteristic (ROC) curve analysis. Additionally, immune cell infiltration in asthma patients was analyzed using the Immune Cell AI database in relation to ferroptosis-related genes. Functional experiments at the cellular level were conducted to assess the effects of key genes on cell viability, inflammation, and ferroptosis. Bioinformatics analysis identified 1,698 DEGs linked to asthma. Five hub genes with clinical diagnostic value— Endothelial PAS Domain Protein 1 (EPAS1), STAT3, G6PD, CYBB, and CBS—were identified. Immune analysis revealed that EPAS1 is closely associated with immune cell infiltration in asthma. Functional experiments further demonstrated that the JAK2/STAT3 axis promotes ferroptosis and inflammatory responses by upregulating EPAS1 expression. Notably, these findings highlight the JAK2/STAT3/EPAS1 axis as a potential therapeutic target for asthma, offering new insights into its molecular mechanisms and identifying novel biomarkers for diagnosis and treatment.

Keywords: Asthma; ferroptosis; JAK2/STAT3; Endothelial PAS Domain Protein 1; EPAS1; inflammation.

INTRODUCTION

The common respiratory condition referred to as asthma is defined by fluctuating airway obstruction, airway hyperreactivity, and persistent inflammation of the airways.[1]. Its clinical manifestations include wheezing, coughing, shortness of breath, and chest tightness[2]. Globally, the incidence of asthma is rising annually, posing a significant public health burden[3]. Genetic predisposition, environmental variables, and aberrant immune system function are all part of the intricate pathophysiology of asthma[4]. Asthma is typically classified into different subtypes, including eosinophilic asthma, neutrophilic asthma, and mixed asthma, based on the predominant inflammatory cell type[5]. Eosinophilic asthma, an important subtype, is primarily driven by the activation of eosinophils and is often associated with more severe disease and poorer prognosis[6]. The biological mechanisms underlying eosinophilic asthma involve the release of cytokines such as interleukin-4 (IL-4), interleukin-5 (IL-5), and interleukin-13 (IL-13), which promote eosinophil recruitment, activation, and survival in the airways[7]. These cytokines, along with other mediators, contribute to airway inflammation, mucus production, and remodeling. Recent studies have identified novel biomarkers for asthma, including fractional exhaled nitric oxide (FeNO), which reflects eosinophilic inflammation in the airways, and epithelial barrier proteins, such as tight junction proteins, which are implicated in the disruption of airway epithelial integrity in asthma[8]. Current treatments for asthma primarily consist of pharmacological interventions and lifestyle modifications, with common medications including inhaled corticosteroids and bronchodilators[9]. Additionally, biologics have emerged as an important treatment option in asthma, particularly for severe and difficult-to-treat cases. Biologic therapies targeting specific molecules involved in the pathogenesis of asthma, such as mepolizumab, benralizumab, omalizumab, reslizumab, and most recently Tezepelumab, have demonstrated efficacy in reducing exacerbations, improving lung function, and decreasing the need for oral corticosteroids[10]. These biologics work by targeting key inflammatory mediators, such as IL-5 and immunoglobulin E (IgE), thus offering a more targeted and personalized approach to asthma management.

A new type of planned cell death called ferroptosis is defined by excessive intracellular iron buildup and lipid peroxidation[11]. This mechanism differs from traditional apoptosis or necrosis, involving abnormal iron deposition and oxidative stress[11]. Recent studies have drawn considerable attention to ferroptosis across various diseases, focusing on mechanisms

such as intracellular iron homeostasis imbalance, lipid peroxidation, and disruption of the antioxidant system[12]. Research on ferroptosis in respiratory diseases has made significant progress. Ferroptosis has a function in controlling chronic obstructive pulmonary disease, where unstable iron accumulation and enhanced lipid peroxidation are observed in lung epithelial cells during cigarette smoke (CS) exposure, accompanied by non-apoptotic cell death[13]. In idiopathic pulmonary fibrosis, Fraxetin alleviates the progression of the disease by inhibiting NCOA4-mediated epithelial cell ferroptosis and reducing inflammatory cytokine release[14]. In asthma, ferroptosis has also been linked to airway remodeling and inflammatory responses[15]. In human airway smooth muscle cells and fibroblasts, elevated iron levels can cause pro-inflammatory cytokine and/or extracellular matrix responses. *In vivo*, elevated iron levels can cause important aspects of asthma, such as airway hyperreactivity, fibrosis, and T2 inflammation[16]. Studies suggest that the ferroptosis inhibitor ferrostatin-1 could improve asthma[17]. Understanding ferroptosis in asthma provides valuable insights into its underlying mechanisms. Targeting ferroptosis pathways in combination with biologic therapies may offer new therapeutic approaches for asthma management.

The Janus kinase 2 (JAK2) /signal transducer and activator of transcription 3 (STAT3) pathway is a key signaling cascade involved in various biological processes such as immune response, inflammation, and cell survival[18]. JAK2 is a tyrosine kinase that, upon activation by cytokines and growth factors, phosphorylates and activates the transcription factor STAT3. Recent study has highlighted that STAT3 acts as a key regulator of ferroptosis in gastric cancer, inhibiting tumor growth and alleviating chemotherapy resistance[19]. Endothelial PAS domain-containing protein 1 (EPAS1), primarily involved in regulating cellular responses to hypoxia, controls processes such as erythropoiesis, angiogenesis, and metabolism[20]. Recent research has also shown that EPAS1 is a hypoxia- and ferroptosis-related gene, particularly in diseases where oxidative stress and iron metabolism are dysregulated[21]. By examining asthma transcriptome data, this work seeks to discover important genes linked to ferroptosis and their enriched pathways. Additionally, it seeks to explore the regulatory mechanism of the JAK2/STAT3/EPAS1 axis on ferroptosis in asthma. We anticipate that this research will deepen our knowledge of the pathophysiology of asthma airway epithelial damage, offer novel targets for asthma therapy, and pave the road for the creation of relevant pharmaceutical agents.

MATERIALS AND METHODS

Data acquisition and differentially expressed genes (DEGs) screening

We first analyzed the genes that play a role in asthma. The GEO database (https://www.ncbi.nlm.nih.gov/geo/) provided the gene expression information for GSE134544. Gene expression profiles from 20 control samples and 41 asthma samples are included in GSE134544. The GEO2R tool was utilized to examine DEGs. Genes deemed upregulated had a fold change (FC) of more than 1.3 and *P*-value less than 0.05. Conversely, downregulated genes were those with *P*-value of less than 0.05 and an FC of less than 0.77.

Enrichment analysis

To explore the potential biological functions of the genes, we performed an enrichment analysis. Three Gene Ontology (GO) domains—Biological Process (BP), Cellular Component (CC), and Molecular Function (MF)—were used for the functional enrichment study. Pathway datasets pertaining to illnesses, medications, chemicals, and biological activities are available in the Kyoto Encyclopedia of Genes and Genomes (KEGG) database. Enrichment analysis was performed using the clusterProfiler (V. 4.8.1) R package to determine the biological functions of genes and associated pathways. The results of the GO and KEGG enrichment analyses were visualized using the online website (http://www.bioinformatics.com.cn/?keywords=pathway).

Weighted gene co-expression network analysis (WGCNA)

To obtain key modules related with asthma, we performed WGCNA analysis. The R package WGCNA (V. 1.71) was utilized to generate the gene co-expression network. First, gene expression data were preprocessed to remove low-expression genes and samples with excessive missing values, followed by normalization to ensure data suitability. A weighted adjacency matrix was built by calculating the Pearson correlation between gene pairs, followed by raising the correlation coefficients to a power (soft-thresholding power, β) to ensure a scale-free network topology. Weighted correlation coefficients were used to build an adjacency matrix, which was subsequently converted into a Topological Overlap Matrix (TOM). Modules were identified using hierarchical clustering, and feature genes were computed. With a merge cut height of 0.25, the soft-thresholding power was set to β = 12. The association between phenotypes (i.e., asthma or control samples) and each module was

evaluated using Pearson correlation analysis, which identified modules linked to asthma. These modules' genes were thought to be asthma-related module genes.

Extraction of ferroptosis-related genes

To analyze the association in ferroptosis and asthma, we obtained ferroptosis-related genes from the FerrDb V2 database. The purpose of the manually curated ferroptosis database FerrDb V2 (http://www.zhounan.org/ferrdb/current/) is to maintain and find ferroptosis-related disorders and biomarkers and regulators[22]. Genes associated with ferroptosis were extracted from this database to undertake the investigation. These genes were contrasted with the WGCNA-derived asthma-related module genes. A Venn diagram (http://bioinformatics.psb.ugent.be/webtools/Venn/) was utilized to show how these genes overlapped.

Interaction network construction and hub gene identification

To analyze the connections between the genes, we constructed the protein-protein interaction (PPI) network. The Search Tool for the Retrieval of Interacting Genes (STRING, https://string-db.org/) was an online tool utilized to investigate protein-protein interaction (PPI) networks. Using Cytoscape V3.9.0 (https://cytoscape.org/), PPI networks with a confidence score higher than 0.40 were chosen and made visually appealing. CytoHubba's calculation of Degree was used to identify hub genes, with the top 10 nodes being regarded as hub genes. An open-source program called GeneMANIA (http://www.genemania.org) is a flexible and easy-to-use tool for creating and displaying interactive functional association networks that show the connections between genes.

Single-gene gene set enrichment analysis (GSEA)

The single-gene GSEA analysis was used to reveal the potential biological functions of the key genes. The correlation coefficient between target gene expression and total gene expression, which served as the GSEA's ranking criterion, was computed in order to run the GSEA. The reference gene sets were the KEGG gene sets. GSEA was performed with the R software package "clusterProfiler." A significance level of P less than 0.05 was used.

Immune infiltration correlation analysis

With gene expression datasets, such as those including RNA-Seq and microarray data, ImmuneCellAI (https://guolab.wchscu.cn/ImmuCellAI/#!/) is a tool for calculating the

abundance of 24 different kinds of immune cells. Six immune cell types and eighteen T cell subtypes make up these twenty-four immune cells. The infiltration levels of these 24 immune cells in control and asthma samples were examined via the ImmuneCellAI algorithm. Pearson correlation coefficients were used to assess the correlation between immune cell infiltration and the correlation between immune cell infiltration and ferroptosis-related genes.

Cell culture and treatment

To investigate the role of key genes, we constructed cellular models of asthma. Dulbecco's Modified Eagle Medium (Gibco, USA) supplemented with 10% fetal bovine serum (FCS500; Excell Bio, China) was used to cultivate human bronchial epithelial cells (16HBE, YS003C, Yaji Bio, China) in an incubator with 5% CO_2 (37°C). Two types of cells were created: IL-13 and control (Ctrl). Interleukin-13 (IL-13; C01M, 10 ng/ml, Nearshore Protein, China) was administered to the IL-13 group for a duration of twenty-four hours to build asthma model[23].

Cell transfection

Subsequently, we investigated the roles of STAT3 and EPAS1 in asthma by overexpressing or knocking down STAT3 and EPAS1. GenePharma (China) created and provided control siRNA (si-NC) and targeted small interfering RNA (siRNA) against STAT3 (si-STAT3). Wuhan Miaoling Biotechnology Co., Ltd. provided the overexpression plasmids for STAT3 (OE-STAT3), endothelial PAS domain protein 1 (EPAS1; OE-EPAS1), and a control plasmid (OE-NC). Eight groups (OE-NC, OE-STAT3, si-NC, si-STAT3, si-NC+OE-NC, si-STAT3+OE-NC, si-NC+OE-EPAS1, and si-STAT3+OE-EPAS1) were created from the 16HBE cells.Following the directions provided by the maker, Lipofectamine 2000 (12566014; Thermo Fisher Scientific, USA) was used to transfect siRNA and overexpression plasmids into 16HBE cells. Following a 48-hour transfection, cells received a 24-hour IL-13 treatment.

5-ethynyl-2'-deoxyuridine (EdU) assay

Next, we analyzed the changes in cell viability in the asthma cell model using the EdU assay. The EdU staining proliferation kit (E-CK-A376; Elabscience, China) was used per what the manufacturer recommends to measure cell proliferation. Following seeding in 4-well plates, 16HBE cells were exposed to 20 µM EdU for a duration of 72 hours. The cells were fixed with 4% paraformaldehyde (P0099; Beyptime, China) after being incubated for two hours.

The ratio served as a quantitative readout of EdU positivity. All photos were processed using Image J software (CA, US) to quantify the fluorescence intensity of the DAPI and GFP channels.

Enzyme-linked immunosorbent assay (ELISA)

ELISA was used to analyze the changes in inflammation levels in the asthma cell model. ELISA was employed to measure the amounts of human interleukin-18 (IL-18; RX106154H, Ruixin Bio, China), interleukin-1β (IL-1β; RX106152H, Ruixin Bio, China), and interleukin-6 (IL-6; RX106126H, Ruixin Bio, China) in cell culture supernatants. A microplate reader was used to determine absorbance (450 nm).

Glutathione (GSH) measurement

A microplate-based reduced GSH assay kit (A006-2-1, Jiancheng Bio, China) was used to assess the levels of GSH. The necessary reagents were produced together with the GSH standard samples, per the manufacturer's instructions. Following centrifugation of the cells in a homogenization buffer mixture, the supernatant was combined with the standard samples and supplied reagents. A microplate reader was then used to detect absorbance (405 nm).

Superoxide dismutase (SOD) activity assay

SOD levels were determined using a test kit (A001-3, Jiancheng Bio, China) following the manufacturer's instructions. Centrifugation was used to gather the cells, and ultrasonication was subsequently used to disrupt them. Using a microplate reader, absorbance (450 nm)was measured to determine the SOD activity in line with the directions provided by the maker.

Malondialdehyde (MDA) measurement

Using an MDA detection kit (A003-1, Jiancheng Bio, China), the levels of MDA were obtained. Using the kit's designated chemicals and cell samples, a mixed solution was created in keeping with the instructions provided by the maker. Samples were chilled and centrifuged at 3500 rpm following incubation. Microplate reader was used to determine absorbance (532 nm).

Ferrous (Fe^{2+}) and ferric (Fe^{3+}) ion measurement

We used a colorimetric iron assay kit (I291, Tongren Chemical, China) to measure the Fe^{2+} and Fe^{3+} levels. Following lysis on ice, the cells were centrifuged at 15000 g. After adding

an iron-reducing reagent to the supernatant, it was incubated for forty minutes. Optical density (593 nm) was determined via microplate reader.

Reactive oxygen species (ROS) measurement

Using a ROS detection kit (BB-47053, Beibo, China), the levels of ROS were determined. Cells were cleaned with Phosphate Buffered Saline (PBS; C0221A, Beyptime, China) following centrifugation and pellet collection. After diluting DCFH-DA (1:1000) in a serum-free medium, the cells were left to develop for 30 minutes(dark 37°C). Cells were rinsed with serum-free media after incubation. Lastly, an inverted fluorescence microscope was used to take fluorescence pictures.

Quantitative real-time polymerase chain reaction (qRT-PCR)

TRIzol reagent (15596018CN, Thermo Fisher Scientific, USA) was applied to get whole RNA. Using a NanoDrop spectrophotometer (Thermo Fisher Scientific, USA) set at 260/280 nm, the quality and amount of RNA were measured. Using a reverse transcription kit (including dsDNase) (BL699A, Biosharp, China), reverse transcription was carried out. Fluorescent real-time PCR equipment (Bio-Rad, USA) and 2×SYBR Green qPCR Master Mix (High ROX) (MPC2208011, Servicebio, China) served for the quantitative PCR. The relative mRNA levels of the target genes were quantified using the $2^{-\Delta\Delta Ct}$ method, with normalization to the internal control β-actin. A list of primers is located in Supplementary Table 1.

Western blot

After collecting the cells, they were lysed for 30 minutes on ice in lysis buffer (BL504A, Biosharp, China). Following a 15-minute centrifugation of the lysates at 12,000 rpm, the supernatant containing total cell protein was recovered. Proteins were separated on polyvinylidene fluoride (PVDF) membranes (IPVH00010, Millipore, Germany) by sodium dodecyl sulfate-polyacrylamide gel electrophoresis (10%, Servicebio, China). The appropriate primary antibodies (Supplementary Table 2)were treated with the membranes for an overnight period at 4°C. The membranes were incubated for 2h (room temperature) with either goat anti-mouse IgG (H + L) (ZB-2305, Zs-BIO, China) or goat anti-rabbit IgG (H + L) HRP (ZB-2301, Zs-BIO, China) following three rounds of TBST washing. A

chemiluminescent reagent (BL520B, Biosharp, China) was used to observe the protein bands, and Image J software was used to quantify the bands.

Transmission electron microscopy

TEM was utilized to investigate alterations in mitochondrial function and cell shape. After trypsinization, the cells were centrifuged and cleaned with PBS. After fixation in 4% paraformaldehyde, a graded ethanol series (64-17-5, Nanjing Reagent, China) was applied for dehydration. The samples were then embedded in epoxy resin (45359-1EA-F, Merck, USA) and sectioned to a thickness of 75 nm. The sections were placed on carbon-coated copper grids and stained with uranyl acetate (SPI-02624, HEAD, China) for 10 minutes, followed by treatment with lead citrate (HD17800, HEAD, China) for an additional 10 minutes. Transmission Electron Microscopy (TEM) (CM-100, Philips, Netherlands) was employed to analyze the samples. Ultrastructural changes in mitochondria in cells observed using TEM provide an important basis for understanding whether iron death occurs in cells.

Statistical analysis

The structural data obtained from the experimental analysis were statistically evaluated for significance and reliability. The correlation analysis was evaluated using Pearson correlation. Using the survivalROC program, receiver operating characteristic (ROC) curves were plotted. To do statistical analysis, GraphPad Prism 8.2.0 was put to use. Student's t-test or one-way analysis of variance (ANOVA) with Tukey's post hoc test was used to compare variables between groups. All results are presented as mean ± standard deviation. *P*-value of < 0.05 was considered statistically significant.

RESULTS

IL-13-induced ferroptosis in 16HBE cells

In the 16HBE cell line, IL-13 treatment significantly inhibited cell proliferation compared to the Ctrl group (Figure 1A). Following IL-13 treatment, there was a substantial rise in IL-1β, IL-6, and IL-18 levels (Figures 1B-1D). Additionally, IL-13 therapy led to higher levels of MDA and ROS and lower levels of SOD and GSH (Figures 2A-2D). Analysis of iron content in 16HBE cells post-IL-13 treatment revealed an increase in Fe^{2+} levels and a drop in Fe^{3+} in contrast to the Ctrl group (Figures 2E-2F). Additionally, IL-13 downregulated the levels of

the ferroptosis marker GPX4 (Figures 2G-2H). Electron microscopy revealed ferroptosis-related abnormalities in mitochondria, including mitochondrial shrinkage, reduced mitochondrial cristae, and outer mitochondrial membrane rupture (Figure 2D).

Functional enrichment analysis of DEGs

To explore the molecular mechanisms in asthma, 1698 DEGs (777 upregulated and 921 downregulated genes) were screened based on GSE134544 (Figure 3A). KEGG pathway and GO enrichment analyses were performed on these DEGs for revealing the potential biological functions of DEGs. The TNF signaling pathway, HIF-1 signaling pathway, and NOD-like receptor signaling pathway were among the pathways where upregulated DEGs were observed to be enriched (Figure 3B). KEGG enrichment analysis also indicated that downregulated DEGs were highly associated with pathways including cellular senescence, T cell receptor signaling pathway, and Th1 and Th2 cell differentiation (Figure 3C). Upregulated DEGs in BP mainly involved IκB kinase/NF-κB signaling, immune response, and inflammation (Figure 3D). In CC, they were linked to cytosol, exosomes, and plasma membrane (Figure 3D). In MF, they were associated with protein binding, actin binding, ATP binding, and kinase activity (Figure 3D). Downregulated DEGs in BP were related to T cell receptor signaling, translation, and cellular defense (Figure 3E). In CC, they were primarily in cytoplasm, nucleoplasm, and ribosomes (Figure 3E). In MF, they were enriched in protein and RNA binding, ribosome structure, and MHC class I binding (Figure 3E). This suggests that DEGs may regulate asthma through these genobiological pathways.

WGCNA analysis and key module identification

WGCNA was used to screen further for key modules related to asthma. Using a soft threshold of 12 ($R^2 = 0.85$), the scale-free network was built(Figures 4A-4B). The adjacency matrix was developed, and TOM was constructed (Figure 4C). Module reliability was confirmed through module correlation analysis (Figure 4D). Correlation analysis between modules and phenotype data identified the blue module as highly associated with asthma (Figure 4E). Therefore, we chose the blue module for subsequent analysis.

Hub gene identification and expression analysis

To analyze whether ferroptosis is involved in asthma, we obtained 472 ferroptosis-related genes based on the FerrDb V2 database. 24 ferroptosis-related genes were identified from

the blue module in the WGCNA analysis (Figure 5A). The PPI network was used to reveal the interactions among 24 ferroptosis-related genes. 24 nodes and 22 edges made up the PPI network (Figure 5B). Figure 5C visually represents the network relationships and degree values of the top 10 key genes (darker colors indicate higher values), including CYBB, EPAS1, CBS, G6PD, MUC1, BRD4, KDM6B, POR, SRC and STAT3. The top 20 most often changed genes associated with the hub genes are shown in the gene-gene interaction network (Figure 5D). The GSE134544 database served to look into the expression levels of these important genes, revealing significant upregulation of SCYBB, EPAS1, CBS, G6PD, MUC1, BRD4, KDM6B, POR, SRC, and STAT3 in asthma compared to the control group (Figures 6A-J). Additionally, we further analyzed the expression correlations among the key genes (Figure 6K).

ROC and GSEA analysis of hub genes

The area under the ROC curve (AUC) can be used to assess the clinical diagnostic value of the genes. As shown in Figure 7, the AUC values of CYBB (AUC=0.82, Figure 7I), EPAS1 (AUC=0.839, Figure 7M), CBS (AUC=0.804, Figure 7E), G6PD (AUC=0.86, Figure 7Q), and STAT3 (AUC=0.873, Figure 7S) indicate high diagnostic accuracy for asthma (AUC > 0.8), whereas MUC1 (AUC=0.777, Figure 7G), BRD4 (AUC=0.687, Figure 7A), KDM6B (AUC=0.7, Figure 7C), POR (AUC=0.749, Figure 7K), and SRC (AUC=0.73, Figure 7O) show lower diagnostic predictive value for asthma. GSEA revealed significant enrichment of BRD4 in ribosome, axon guidance and glycerolipid metabolism (Figure 7B). KDM6B was significantly enriched in antigen processing and presentation and FC gamma receptor-mediated phagocytosis (Figure 7D). CBS was significantly enriched in FC gamma receptor-mediated phagocytosis and RNA degradation (Figure 7F). MUC1 was significantly enriched in ribosome and GnRH signaling pathway (Figure 7H). CYBB was significantly enriched in ribosome and sulfur metabolism (Figure 7J). POR was significantly enriched in GnRH signaling pathway and ribosome (Figure 7L). EPAS1 was significantly enriched in the Fc epsilon RI signaling pathway and GnRH signaling pathway (Figure 7N). SRC was significantly enriched in GnRH signaling pathway and calcium signaling pathway (Figure 7P). G6PD was significantly enriched in ribosome and nucleotide excision repair (Figure 7R). STAT3 was significantly enriched in oxidative phosphorylation and FC gamma receptor-mediated phagocytosis (Figure 7T). In conclusion, CYBB, EPAS1, CBS, G6PD, and STAT3 hold diagnostic value in asthma.

Correlation analysis of immune infiltration in asthma

To evaluate changes in the immune microenvironment in asthma, we conducted an immune analysis. The GSE134544 dataset's infiltration of 24 different immune cell types was examined (Figure 8A). Thirteen immune cell types showed significant variations in infiltration within asthma and control groups. Specifically, the group with asthma showed elevated levels of monocytes, macrophages, neutrophils, and nTreg cells, while the control group had higher levels of NK cells, CD4$^+$ T cells, CD8$^+$ T cells, gamma-delta T cells, iTreg cells, Th2 cells, Tfh cells, exhausted T cells, and effector memory T cells (Figure 8B). Further analysis of immune cell infiltration in asthma showed various correlations between cells (Figure 8C). There was the greatest positive association found between CD8$^+$ T cells and Tex cells (0.82), followed by neutrophils and monocytes (0.61), and Tex cells and NK cells (0.60). Conversely, the strongest competitive effect was observed between Tgd cells and Th17 cells (-0.63), followed by Tgd cells and neutrophils (-0.57), and neutrophils and CD8$^+$ T cells (-0.55). Figure 8D displays the positive/negative links among immune cells and important genes. CBS was adversely connected with MAIT cells. CYBB was favorably linked to Th17 cells and neutrophils, but adversely connected with Th1 cells, exhausted T cells, Tfh cells, iTreg cells, NK cells, Tgd cells, DC cells, NKT cells, and CD8$^+$ T cells. EPAS1 was adversely connected with MAIT cells, Tfh cells, Tex cells, CD8$^+$ T cells, and NK cells. G6PD was adversely connected with Tcm cells, Tex cells, Tfh cells, NK cells, and CD8$^+$ T cells, but favorably linked to B cells. STAT3 was adversely connected with Tex cells, Tfh cells, DC cells, NK cells, CD4$^+$ T cells, and CD8$^+$ T cells, but favorably linked to macrophages and neutrophils. This suggests that key ferroptosis-related genes may regulate asthma by modulating immune cell infiltration.

JAK2/STAT3 regulates ferroptosis and inflammatory reaction induced by IL-13 in 16HBE cells

Bioinformatics analyses identified STAT3 as a key gene related to ferroptosis in asthma. Prior research suggests that JAK2/STAT3 has an impact in initiating and developing inflammatory and immune responses in various pathological conditions, playing significant roles in multiple diseases[24]. QRT-PCR results revealed that IL-13 treatment led to increased mRNA levels of JAK2 and STAT3 (Figure 9A-9B). This was confirmed by Western blotting, which demonstrated elevated protein levels of JAK2, p-STAT3, and STAT3 upon IL-13 treatment (Figure 9C-9F). We effectively knocked down or

13

overexpressed STAT3 in 16HBE cells by siRNA or overexpression plasmids (Figure 9G-9H). Among these, si-STAT3#2 exhibited the highest knockdown efficiency and was used for subsequent experiments. EdU assays demonstrated that STAT3 overexpression significantly inhibited cell viability, while STAT3 knockdown significantly increased it (Figure 9I-9J). ELISA results showed that STAT3 promotes the increase of IL-6, IL-18, and IL-1β in IL-13-induced 16HBE cells (Figure 9K-9M). Further experiments indicated that STAT3 inhibition lowered the GSH, SOD, Fe^{3+} and GPX4, and raised the MDA, ROS, and Fe^{2+} in IL-13-induced 16HBE cells (Figure 10A-10H). The OE-STAT3 group showed increased outer membrane rupture, decreased cristae, and shrinkage of the mitochondria, according to electron microscopy studies, while STAT3 knockdown protected mitochondrial morphology (Figure 10I).

IL-13 upregulates EPAS1 expression via JAK2/STAT3 to regulate ferroptosis and inflammatory reaction in 16HBE cells

A number of malignancies are linked to dysregulation of EPAS1 expression, which also controls ferroptosis in clear cell and cervical cancers[21]. IL-13 treatment increased EPAS1 levels (Figure 11A-11B). Notably, previous PPI network analysis indicated an interaction between STAT3 and EPAS1. We further explored the correlation between STAT3 and EPAS1 expression and found that STAT3 positively regulates EPAS1 expression without affecting JAK2 levels (Figure 11C-11J). We constructed an OE-EPAS1 plasmid for overexpressing EPAS1 in 16HBE cells. Results showed that OE-EPAS1 stopped the decline in EPAS1 levels caused by STAT3 knockdown (Figure 12A, 12D-12E). Knockdown of STAT3 or overexpression of EPAS1 did not significantly alter JAK2 expression (Figure 12B, 12D, 12F). Overexpression of EPAS1 did not significantly affect STAT3 or p-STAT3 levels (Figure 12C, 12D, 12G-12H). When 16HBE cells in the si-STAT3+OE-NC group were juxtaposed to the si-NC+OE-NC group, they had higher cell viability and lower levels of IL-1β, IL-6, and IL-18, while the si-NC+OE-EPAS1 group showed the opposite results (Figure 12I-12L). Cell viability in the si-STAT3+OE-EPAS1 group was higher than in the si-NC+OE-EPAS1 group, but lower than in the si-STAT3+OE-NC group (Figure 12I). The si-STAT3+OE-EPAS1 group had higher doses of IL-1β, IL-6, and IL-18 than the si-STAT3+OE-NC group, but not as high as the si-NC+OE-EPAS1 group (Figure 12J-12L). As opposed to si-NC+OE-NC group, the si-STAT3+OE-NC group showed increased levels of GSH, SOD, Fe^{3+}, and GPX4, and decreased levels of MDA, ROS, and Fe^{2+}, while the si-

NC+OE-EPAS1 group exhibited the opposite results (Figure 13A-13H). Lower than in the si-STAT3+OE-NC group, but greater than in the si-NC+OE-EPAS1 group, were the levels of GSH, SOD, Fe^{3+}, and GPX4 (Figure 13A-13H). The TME results showed that whereas mitochondrial damage was worsened in the si-NC+OE-EPAS1 group, it was lessened in the si-STAT3+OE-NC group in regard to the si-NC+OE-NC group (Figure 13I). More mitochondrial damage than in the si-STAT3+OE-NC group, but less than in the si-NC+OE-EPAS1 group, was seen in the si-STAT3+OE-EPAS1 group (Figure 13A-13H).

DISCUSSION

Bioinformatics is a discipline that uses computational techniques and statistical methods to analyze, process, and interpret biological data, with the aim of uncovering the underlying principles of biological processes. In recent years, bioinformatics has played a pivotal role in elucidating the molecular mechanisms of diseases and identifying potential biomarkers through big data analysis. Liao et al. integrated machine learning and bioinformatics to identify ABHD5 as a lipid-related biomarker in idiopathic pulmonary fibrosis[25]. Liu et al. applied bioinformatics analysis and machine learning to identify six immune-related hub genes in atherosclerosis with rheumatoid arthritis[26]. Additionally, Liao et al. combined bioinformatics and experimental validation to demonstrate that SPP1 is a key regulator of the PI3K/AKT signaling pathway in pulmonary fibrosis[27]. Through bioinformatics analysis, we identified 1698 DEGs associated with asthma. DEGs were highly abundant in Th1 and Th2 cell differentiation, TNF signaling pathway, and HIF-1 signaling pathway. Previous studies have demonstrated that vitamin D improves asthma-induced lung damage by modulating the HIF-1α signaling pathway[28]. An essential component of the TNF signaling system, TNF-α, is essential for asthma inflammation[29]. Anti-TNF-α treatment has been shown to improve lung function, airway hyperreactivity, and quality of life in asthma patients, while also reducing the frequency of acute exacerbations[30]. An imbalance between Th1 and Th2 cells is a major immune abnormality in asthma, with cytokine levels in the serum regulated by Th1/Th2 differentiation in the lungs of asthma patients[31, 32]. These findings highlight the crucial roles of Th1/Th2 immune responses, the TNF signaling pathway, and the HIF-1 signaling pathway in the pathogenesis of asthma, and suggest potential new biomarkers and therapeutic targets for asthma treatment.

Important genes for ferroptosis and asthma were found in our investigation, including EPAS1, STAT3, G6PD, CYBB, and CBS. CYBB, a subunit of NADPH oxidase, plays a role

in endogenous oxidative stress[33]. Mycobacterium leprae promotes macrophage ferroptosis through CYBB, aiding its survival[34]. In mesenchymal glioblastoma, CYBB regulates temozolomide (TMZ) resistance via the ferroptosis-regulating Nrf2/SOD2 axis[35]. G6PD, a key enzyme in glycolysis, is involved in generating reduced glutathione and NADPH, which are crucial for combating oxidative stress[36]. In hepatocellular carcinoma, G6PD inhibits ferroptosis by targeting cytochrome P450 reductase, thereby promoting cell growth, metastasis, and tumorigenesis[37]. CBS, a critical enzyme in sulfur amino acid metabolism, participates in cysteine synthesis and sulfur metabolism[38]. Apolipoprotein C1 promotes glioblastoma development by inhibiting ferroptosis through reduced CBS activity and increased GSH synthesis[39]. These findings highlight the potential roles of EPAS1, STAT3, G6PD, CYBB, and CBS in asthma, possibly through the regulation of ferroptosis, and provide new targets for further research.

We found that 16HBE cells undergo ferroptosis and inflammation when exposed to IL-13. Notably, JAK2/STAT3 expression in 16HBE cells rises by IL-13. STAT3, a key oncogene with dual functions in signal transduction and transcriptional activation, has been shown to be a positive regulator of ferroptosis in pancreatic ductal adenocarcinoma (PDAC) cell lines[40]. In breast cancer, STAT3 increases ACSL4 expression, triggering ferroptosis. In ulcerative colitis (UC) cell models, the phosphorylation level of STAT3 is downregulated, while ferroptosis inhibitor Fer-1 can reactivate STAT3 phosphorylation[41]. STAT3 signaling promotes ferroptosis in high-fat diet-fed mice by upregulating NCOA4-mediated ferritinophagy, leading to cardiac damage[42]. Our experimental results confirm that STAT3 enhances IL-13-induced inflammation and ferroptosis. One important intracellular signaling system involved in many biological processes is the JAK2/STAT3 signaling pathway[43]. In liver cancer, JAK2/STAT3 induces autophagy[44]. The histone deacetylase inhibitor trichostatin A (TSA) reduces JAK2/STAT3 signaling, leading to G1 phase arrest and subsequent apoptosis in colorectal cancer (CRC) cells[45]. Li et al. found that FANCD2 inhibits ferroptosis in osteosarcoma by regulating the JAK2/STAT3 pathway, promoting osteosarcoma cell viability, migration, invasion, and tumor growth[46]. This suggests that IL-13 may exacerbate ferroptosis and inflammation by upregulating JAK2/STAT3, inducing damage in 16HBE cells and promoting asthma development.

The cytokine EPAS1 was initially cloned in 1997 and has a bHLH-PAS domain[47]. The placenta, heart, lungs, and endothelial cells are the main organs where EPAS1 is expressed.

16

It is crucial for cancer, angiogenesis, hematopoiesis, and energy metabolism[48]. Research has demonstrated that via upregulating hypoxia-induced lipid droplet-associated expression, EPAS1 induces ferroptosis in clear cell carcinoma.[49]. D-mannose regulates ferroptosis via EPAS1 to alleviate osteoarthritis progression[50]. According to our research, EPAS1 expression in 16HBE cells is stimulated by IL-13. Bioinformatics analysis and experimental validation showed that STAT3 positively regulates EPAS1 expression. Further experiments demonstrated that STAT3 promotes IL-13-induced ferroptosis and inflammation in 16HBE cells by upregulating EPAS1. In a nutshell, IL-13 may exacerbate ferroptosis and inflammation by upregulating JAK2/STAT3 and EPAS1, thereby inducing damage in 16HBE cells and contributing to asthma progression.

This study has several limitations that need to be acknowledged. First, the experiments were conducted exclusively in the 16HBE cell line, limiting the generalizability of the findings to other cell types. Second, while the study focused on GPX4 as a key ferroptosis marker, other important ferroptosis-related genes, such as SLC7A11 and ACSL4, were not examined, which may restrict the understanding of the broader ferroptosis mechanism. Third, the specific phosphorylation sites of JAK2 and STAT3 and their precise regulatory effects on EPAS1 expression, inflammation, and ferroptosis were not analyzed. Additionally, the study lacks functional validation to determine whether the inhibition of JAK2, STAT3, and p-STAT3 can fully reverse IL-13-induced EPAS1 upregulation, inflammation, and ferroptosis. Lastly, the study did not include the assessment of lipid-ROS levels and GSH/GSSG ratios, which are critical for a comprehensive evaluation of oxidative stress during ferroptosis. Future studies addressing these aspects will help to enhance the robustness and applicability of the findings.

CONCLUSION

The important significance of the JAK2/STAT3-EPAS axis in asthma is revealed by this work, which combines experimental validation with bioinformatics analysis. Bioinformatics analysis identified STAT3 and EPAS as key genes closely related to ferroptosis, with their expression significantly upregulated in asthma and positively correlated with each other. Functional experiments confirmed that the JAK2/STAT3 pathway promotes IL-13-induced ferroptosis and inflammation in 16HBE cells by upregulating EPAS1 expression. These findings underscore the importance of this research in uncovering novel molecular

mechanisms of asthma, suggesting potential therapeutic targets for the treatment of asthma through modulation of the JAK2/STAT3-EPAS axis and ferroptosis regulation.

ACKNOWLEDGMENTS

REFERENCES

1.   Bakakos, A., et al., Asthma with fixed airflow obstruction: from fixed to personalized approach. Journal of Personalized Medicine, 2022. 12(3): p. 333.

2.   Sahrun, S., K. Auliya, and K. Sulyastuty, A Case Report of Bronchial Asthma in a 56-Year-Old Mother With the Main Complaint of Shortness of Breath in the Emergency Room. Jurnal EduHealth, 2024. 15(01): p. 784-792.

3.   Yang, C.-h., et al., Global burden of asthma in young adults in 204 countries and territories, 1990‑2019: Systematic analysis of the Global burden of disease study 2019. Preventive Medicine Reports, 2024. 37: p. 102531.

4.   Hizawa, N., The understanding of asthma pathogenesis in the era of precision medicine. Allergology International, 2023. 72(1): p. 3-10.

5.   Zhou, B.-w., H.-m. Liu, and X.-h. Jia, The role and mechanisms of traditional Chinese medicine for airway inflammation and remodeling in asthma: overview and progress. Frontiers in Pharmacology, 2022. 13: p. 917256.

6.   Kawamatawong, T., et al., Guidelines for the management of asthma in adults: evidence and recommendations. Asian Pacific Journal of Allergy and Immunology, 2022. 40(1): p. 1-21.

7.   Yu, Y., et al., Ferroptosis: a cell death connecting oxidative stress, inflammation and cardiovascular diseases. Cell death discovery, 2021. 7(1): p. 193.

8.   Long, H., et al., Iron homeostasis imbalance and ferroptosis in brain diseases. MedComm, 2023. 4(4): p. e298.

9.   Yoshida, M., et al., Involvement of cigarette smoke-induced epithelial cell ferroptosis in COPD pathogenesis. Nat Commun, 2019. 10(1): p. 3145.

10. Zhai, X., et al., Fraxetin alleviates BLM-induced idiopathic pulmonary fibrosis by inhibiting NCOA4-mediated epithelial cell ferroptosis. Inflamm Res, 2023. 72(10-11): p. 1999-2012.

11. Li, M., et al., Ferroptosis triggers airway inflammation in asthma. Therapeutic Advances in Respiratory Disease, 2023. 17: p. 17534666231208628.

12. Ali, M.K., et al., Crucial role for lung iron level and regulation in the pathogenesis and severity of asthma. European Respiratory Journal, 2020. 55(4).

13. Ali, M.K., et al., Crucial role for lung iron level and regulation in the pathogenesis and severity of asthma." M.K. Ali, R.Y. Kim, A.C. Brown et al. Eur Respir J 2020; 55: 1901340. Eur Respir J, 2022. 60(3).

14. Zhou, N., et al., FerrDb V2: update of the manually curated database of ferroptosis regulators and ferroptosis-disease associations. Nucleic acids research, 2023. 51(D1): p. D571-D582.

15. Yang, N. and Y. Shang, Ferrostatin‐1 and 3‐Methyladenine Ameliorate Ferroptosis in OVA‐Induced Asthma Model and in IL‐13‐Challenged BEAS‐2B Cells. Oxidative medicine and cellular longevity, 2022. 2022(1): p. 9657933.

16. Huang, B., X. Lang, and X. Li, The role of IL-6/JAK2/STAT3 signaling pathway in cancers. Frontiers in oncology, 2022. 12: p. 1023177.

17. Lu, X., et al., EPAS1, a hypoxia- and ferroptosis-related gene, promotes malignant behaviour of cervical cancer by ceRNA and super-enhancer. J Cell Mol Med, 2024. 28(9): p. e18361.

18. Huang, C., et al., Vitamin D ameliorates asthma-induced lung injury by regulating HIF-1α/Notch1 signaling during autophagy. Food Sci Nutr, 2022. 10(8): p. 2773-2785.

19.   Xue, K., et al., Panax notoginseng saponin R1 modulates TNF-α/NF-κB signaling and attenuates allergic airway inflammation in asthma. International Immunopharmacology, 2020. 88: p. 106860.

20.   Aldhalmi, A.K., A.J.H. Al-Athari, and H.A.-A.M. Al-Hindy, Association of Tumor Necrosis Factor-α and Myeloperoxidase enzyme with Severe Asthma: A comparative study. Reports of biochemistry & molecular biology, 2022. 11(2): p. 238.

21.   Luo, W., et al., Distinct spatial and temporal roles for Th1, Th2, and Th17 cells in asthma. Frontiers in Immunology, 2022. 13: p. 974066.

22.   Li, Q., et al., Ginsenoside Rh1 attenuates ovalbumin-induced asthma by regulating Th1/Th2 cytokines balance. Bioscience, Biotechnology, and Biochemistry, 2021. 85(8): p. 1809-1817.

23.   Su, I.-C., et al., NADPH oxidase subunit CYBB confers chemotherapy and ferroptosis resistance in mesenchymal glioblastoma via nrf2/SOD2 modulation. International journal of molecular sciences, 2023. 24(9): p. 7706.

24.   Wang, Z., et al., CYBB-Mediated Ferroptosis Associated with Immunosuppression in Mycobacterium leprae-Infected Monocyte-Derived Macrophages. J Invest Dermatol, 2024. 144(4): p. 874-887.e2.

25.   Su, I.C., et al., NADPH Oxidase Subunit CYBB Confers Chemotherapy and Ferroptosis Resistance in Mesenchymal Glioblastoma via Nrf2/SOD2 Modulation. Int J Mol Sci, 2023. 24(9).

26.   Meng, Q., et al., Recent findings in the regulation of G6PD and its role in diseases. Frontiers in Pharmacology, 2022. 13: p. 932154.

27.   Cao, F., A. Luo, and C. Yang, G6PD inhibits ferroptosis in hepatocellular carcinoma by targeting cytochrome P450 oxidoreductase. Cell Signal, 2021. 87: p. 110098.

28.   Zuhra, K., et al., Cystathionine-β-synthase: molecular regulation and pharmacological inhibition. Biomolecules, 2020. 10(5): p. 697.

29.   Zheng, X.-j., et al., Apolipoprotein C1 promotes glioblastoma tumorigenesis by reducing KEAP1/NRF2 and CBS-regulated ferroptosis. Acta Pharmacologica Sinica, 2022. 43(11): p. 2977-2992.

30.   Zhang, W., et al., Thiostrepton induces ferroptosis in pancreatic cancer cells through STAT3/GPX4 signalling. Cell Death & Disease, 2022. 13(7): p. 630.

31.   Huang, F., et al., STAT3-mediated ferroptosis is involved in ulcerative colitis. Free Radic Biol Med, 2022. 188: p. 375-385.

32.   Zhu, M., et al., STAT3 signaling promotes cardiac injury by upregulating NCOA4-mediated ferritinophagy and ferroptosis in high-fat-diet fed mice. Free Radical Biology and Medicine, 2023. 201: p. 111-125.

33.   Hu, Q., et al., JAK/STAT pathway: Extracellular signals, diseases, immunity, and therapeutic regimens. Frontiers in Bioengineering and Biotechnology, 2023. 11: p. 1110765.

34.   Yu, Z., D. Wang, and Y. Tang, PKM2 promotes cell metastasis and inhibits autophagy via the JAK/STAT3 pathway in hepatocellular carcinoma. Molecular and Cellular Biochemistry, 2021. 476(5): p. 2001-2010.

35.   Xiong, H., et al., Trichostatin A, a histone deacetylase inhibitor, suppresses JAK2/STAT3 signaling via inducing the promoter-associated histone acetylation of SOCS1 and SOCS3 in human colorectal cancer cells. Mol Carcinog, 2012. 51(2): p. 174-84.

36.   Li, X. and J. Liu, FANCD2 inhibits ferroptosis by regulating the JAK2/STAT3 pathway in osteosarcoma. BMC Cancer, 2023. 23(1): p. 179.

37.   Tian, H., S.L. McKnight, and D.W. Russell, Endothelial PAS domain protein 1 (EPAS1), a transcription factor selectively expressed in endothelial cells. Genes Dev, 1997. 11(1): p. 72-82.

38.   Chen, H., et al., The potential role of hypoxia-inducible factor-1 in the progression and therapy of central nervous system diseases. Current Neuropharmacology, 2022. 20(9): p. 1651.

39.   Lu, X., et al., EPAS1, a hypoxia‐ and f erroptosis‐related gene, promotes malignant behaviour of cervical cancer by ceRNA and super‐enhancer. Journal of Cellular and Molecular Medicine, 2024. 28(9): p. e18361.

40.   Zhou, X., et al., D‐mannose alleviates osteoarthritis progression by inhibiting chondrocyte ferroptosis in a HIF‐2α‐dependent manner. Cell Proliferation, 2021. 54(11): p. e13134.

FIGURES WITH LEGENDS
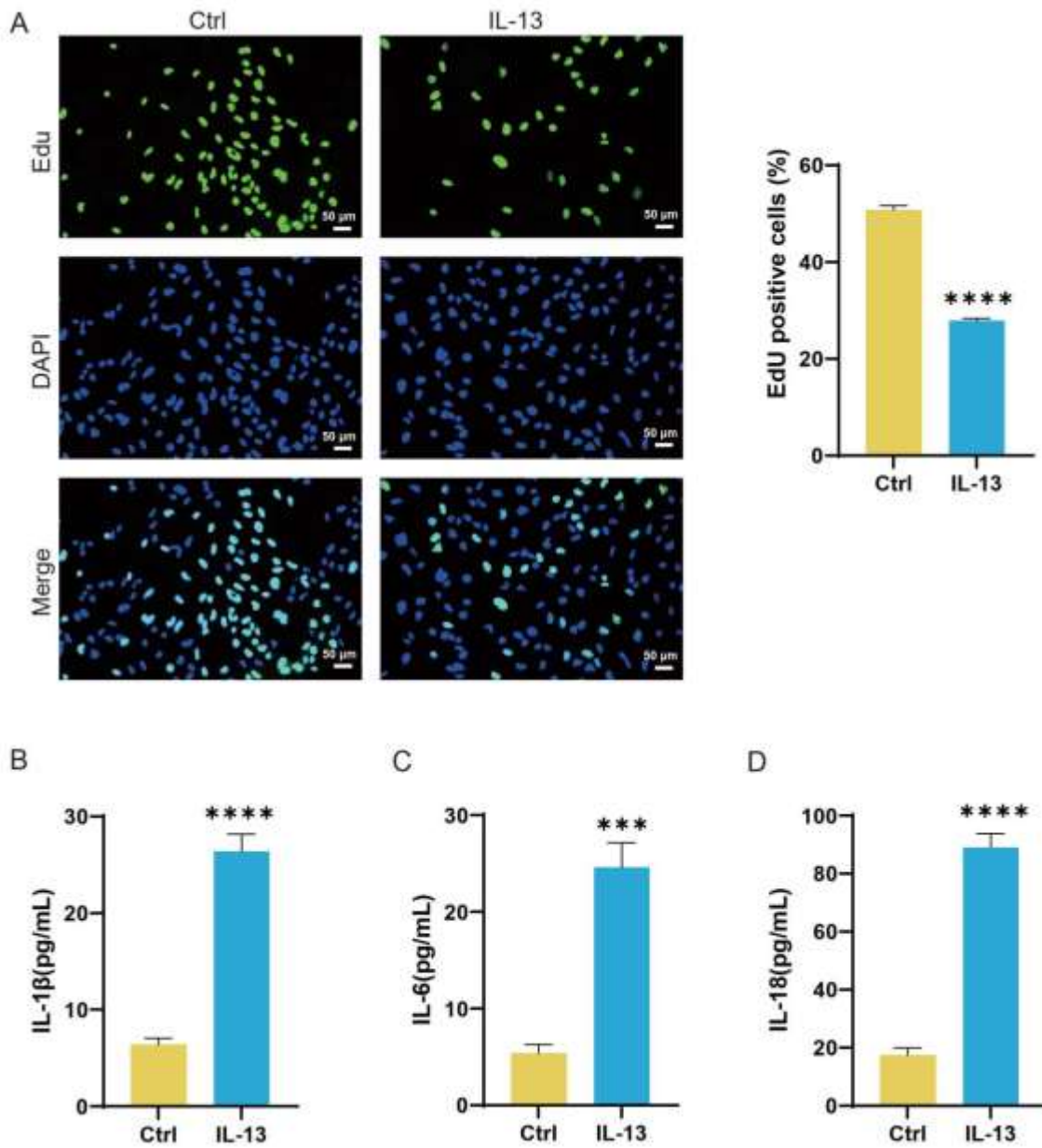
Figure 1. IL-13 Inhibits 16HBE cell proliferation and induces inflammation

(A) Representative results and quantitative analysis of 5-Ethynyl-2'-deoxyuridine (EDU)

staining in 16HBE cells from the Control (Ctrl) and IL-13 groups. EDU-positive cells

(green) are labeled, and cell nuclei are stained with 4',6-diamidino-2-phenylindole (DAPI)

(blue). (B-D) Enzyme-linked immunosorbent assay (ELISA) measurements of interleukin-

1β (IL-1β) (B), interleukin-6 (IL-6) (C), and interleukin-18 (IL-18) (D) levels in 16HBE c
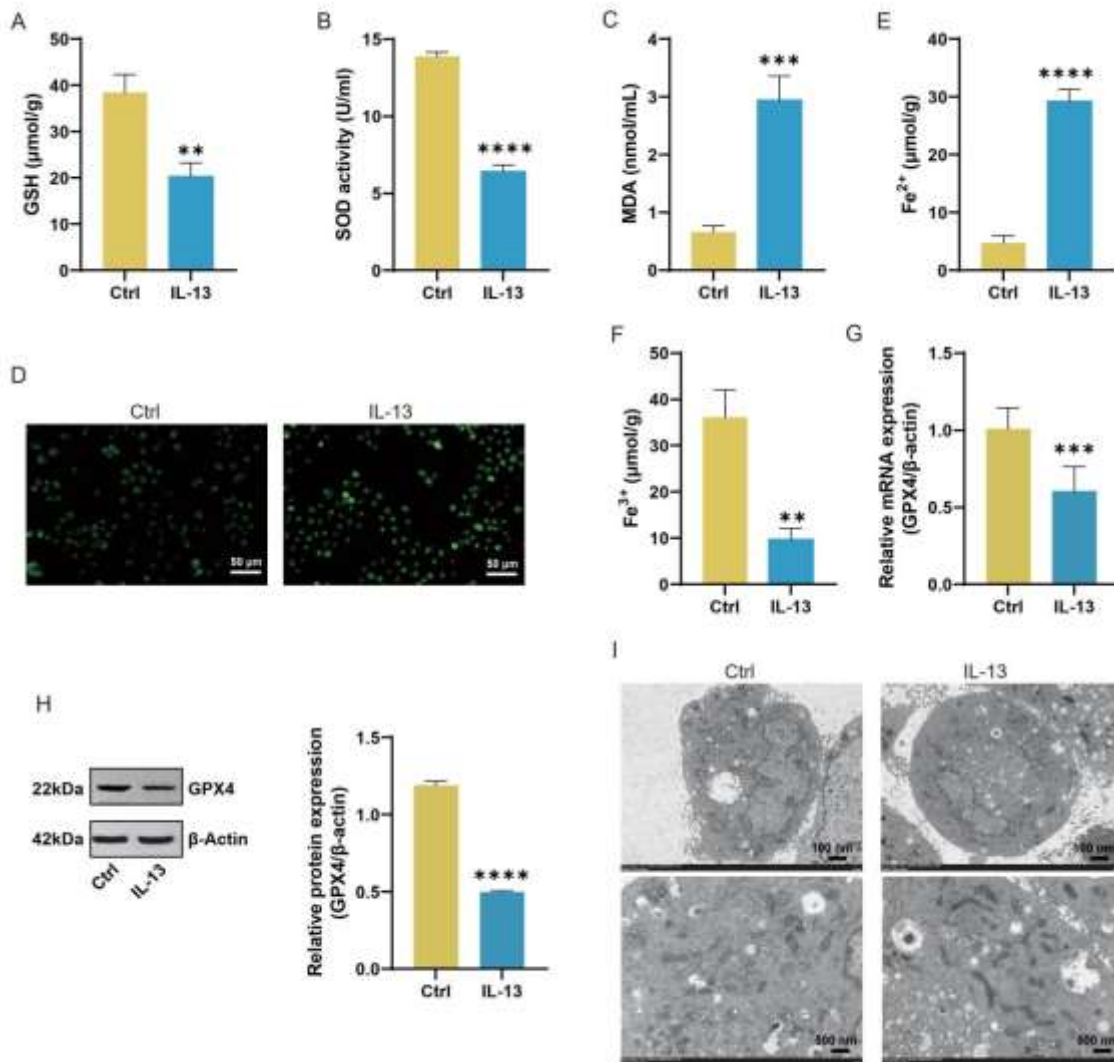
ells from the Ctrl and IL-13 groups. $^{***}P<0.001$, $^{****}P<0.0001$.

Figure 2. IL-13 induces ferroptosis in 16HBE cells

(A-F) Assay kit measurements of glutathione (GSH) (A), superoxide dismutase (SOD) (B), malondialdehyde (MDA) (C), reactive oxygen species (ROS) (D), Fe^{2+} (E), and Fe^{3+} (F) levels in 16HBE cells from the Ctrl and IL-13 groups. (G) Quantitative real-time polymerase chain reaction (qRT-PCR) analysis of glutathione peroxidase 4 (GPX4) mRNA levels in 16HBE cells from the Ctrl and IL-13 groups. (H) Western blotting (WB) analysis of GPX4 protein levels in 16HBE cells from the Ctrl and IL-13 groups. (I) Transmission

electron microscopy (TEM) images showing mitochondrial morphology in 16HBE cells from the Ctrl and IL-13 groups. $^{**}P<0.01$, $^{***}P<0.001$, $^{****}P<0.0001$.
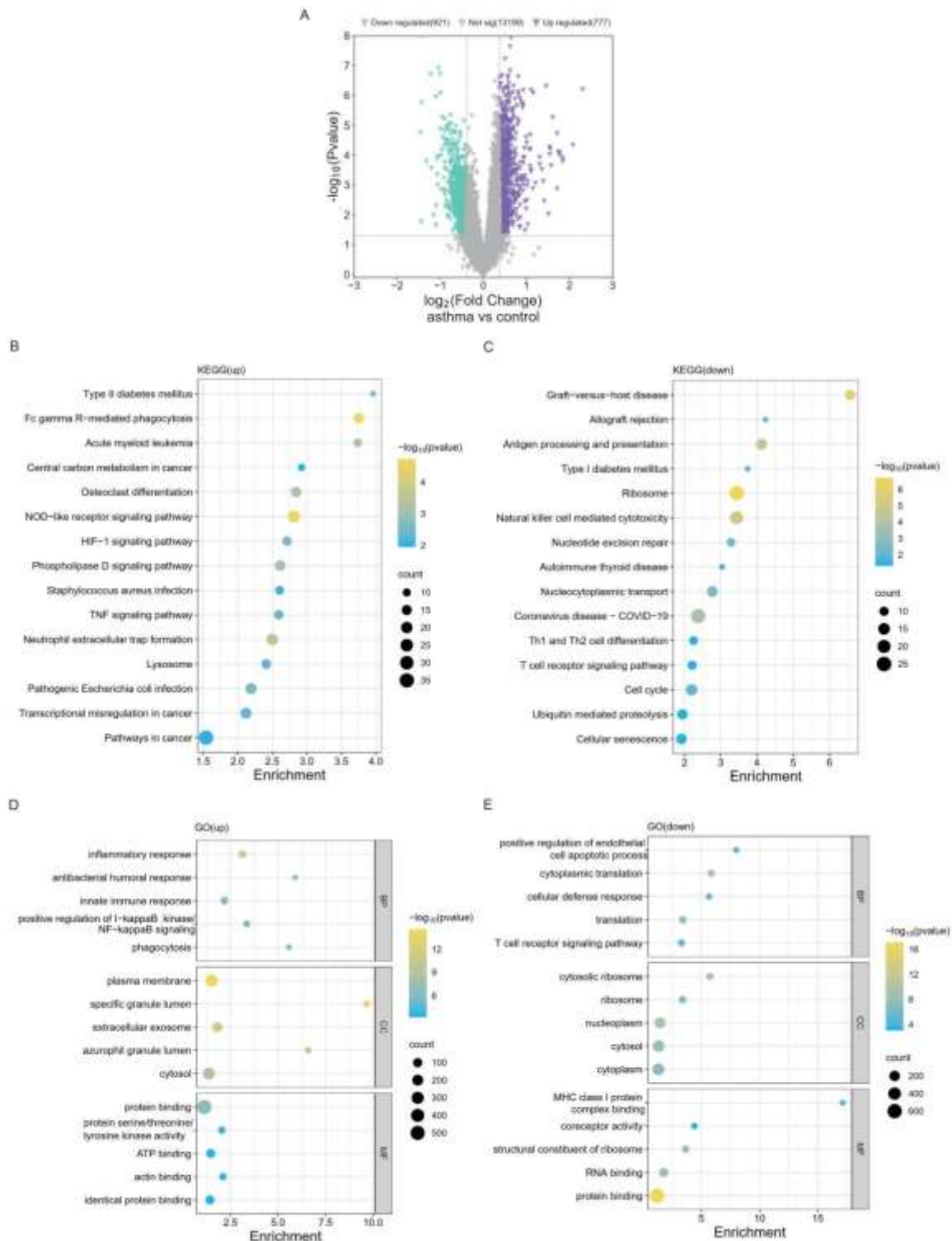
**Figure 3. Differential expression analysis and functional enrichment analysis**

(A) Volcano plot of differentially expressed genes (DEGs) in asthma from the GSE134544 dataset. Purple represents upregulated genes, and green represents downregulated genes. (B) Kyoto Encyclopedia of Genes and Genomes (KEGG) enrichment analysis of upregulated DEGs. (C) KEGG enrichment analysis of downregulated DEGs. (D) Gene Ontology (GO) enrichment analysis of upregulated DEGs. (E) GO enrichment analysis of downregulated DEGs.
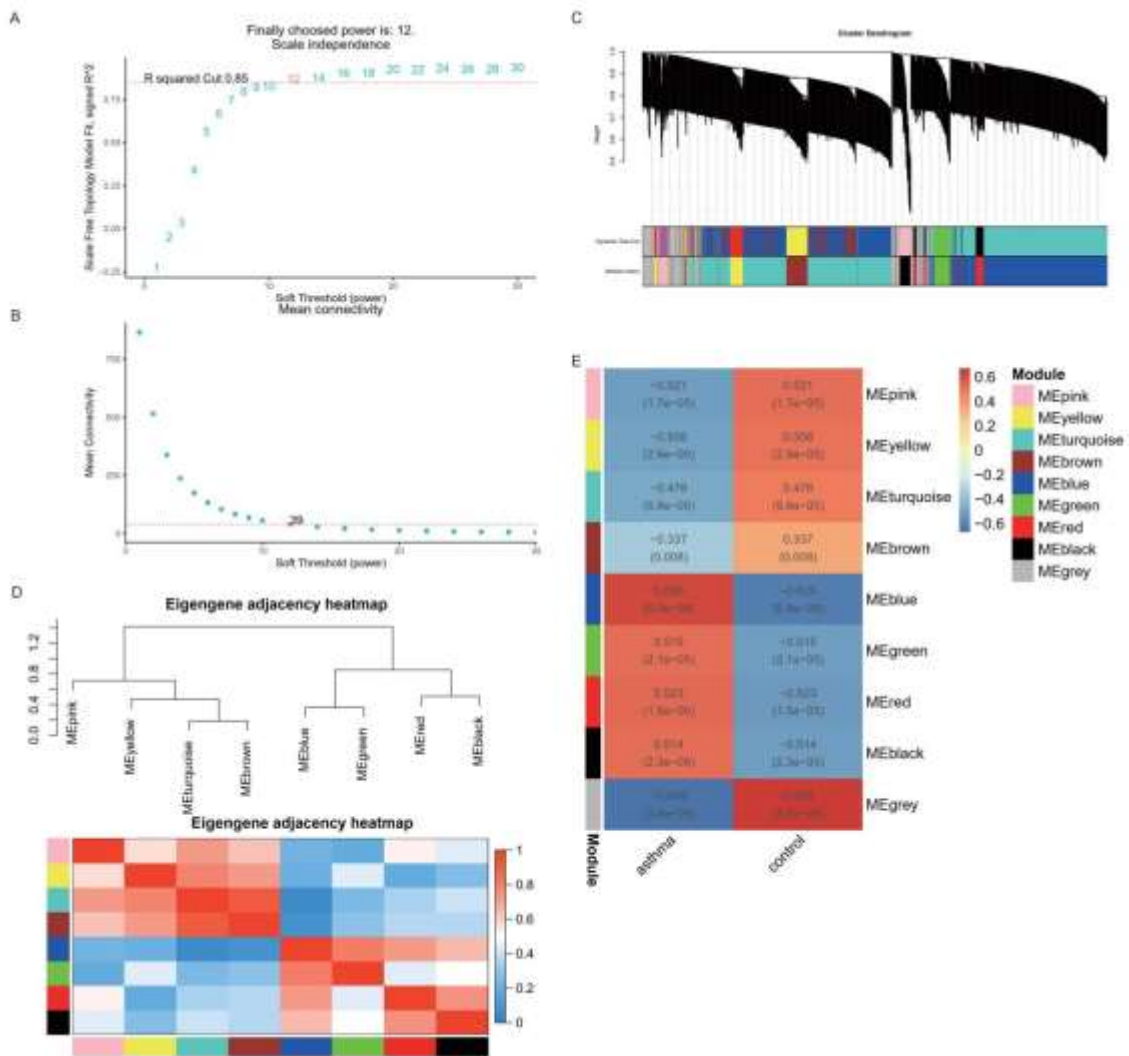

Figure 4. WGCNA and core module identification

(A) Analysis of the scale-free index (β) for various soft-threshold powers. (B) Analysis of the mean connectivity for various soft-threshold powers. (C) Gene clustering dendrogram

based on topological overlap and assigned module colors. (D) Heatmap of feature gene

adjacency for the eight modules. (E) Heatmap showing the correlation between each

module's feature genes and phenotypes.
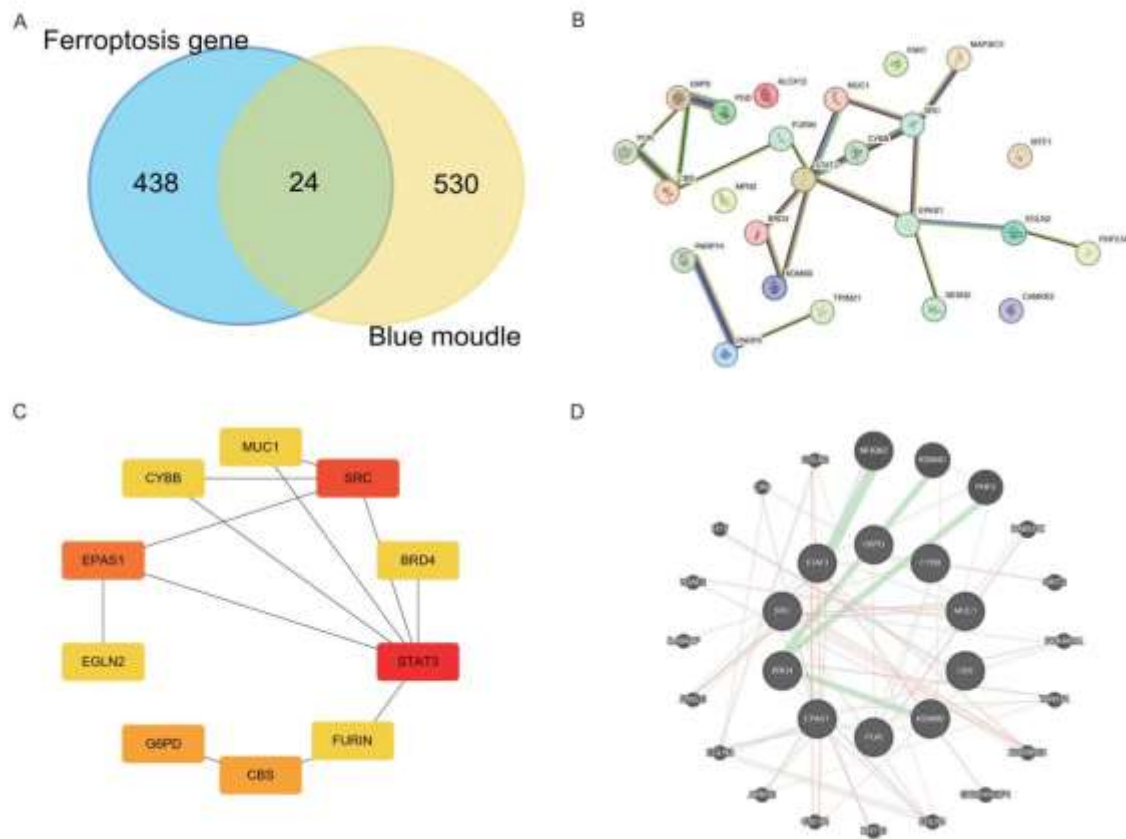
Figure 5. Interaction network construction and hub gene identification

(A) Venn diagram showing overlapping genes between asthma-related module genes and

ferroptosis-related genes. (B) Protein-protein interaction (PPI) network of overlapping

genes. Edges between nodes represent gene-gene interactions. (C) PPI network of the top

10 hub genes based on degree. (D) Gene-gene interaction network of the top 10 hub genes.
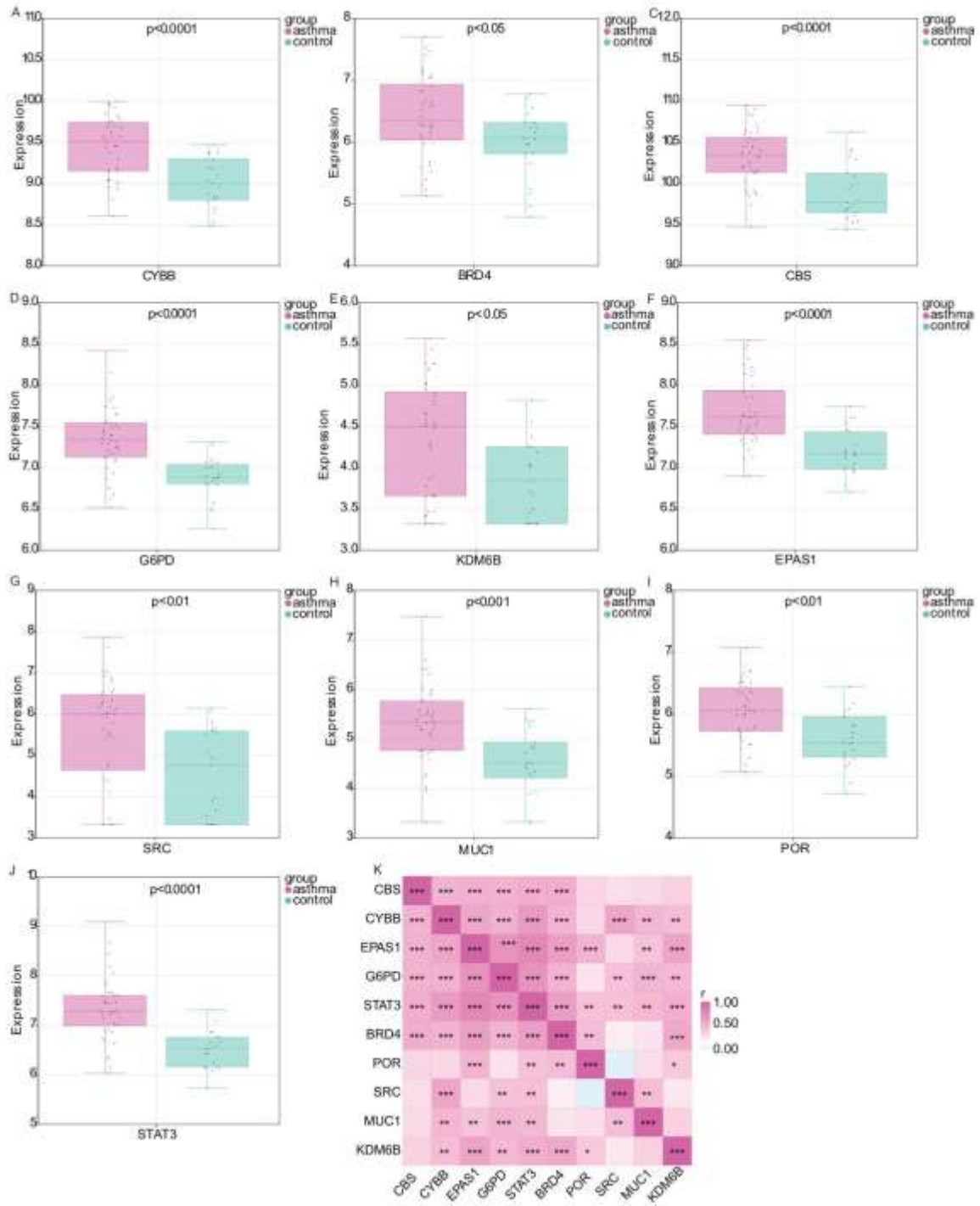
Figure 6. Expression levels and correlation analysis of hub genes

Expression levels of CYBB (A), BRD4 (B), CBS (C), G6PD (D), KDM6B (E), EPAS1 (F), SRC (G), MUC1 (H), POR (I), and STAT3 (J) in asthma and control samples based on the GSE134544 database. (K) Pearson correlation analysis of the relationships between hub genes. [*]$P<0.05$, [**]$P<0.01$, [***]$P<0.001$.
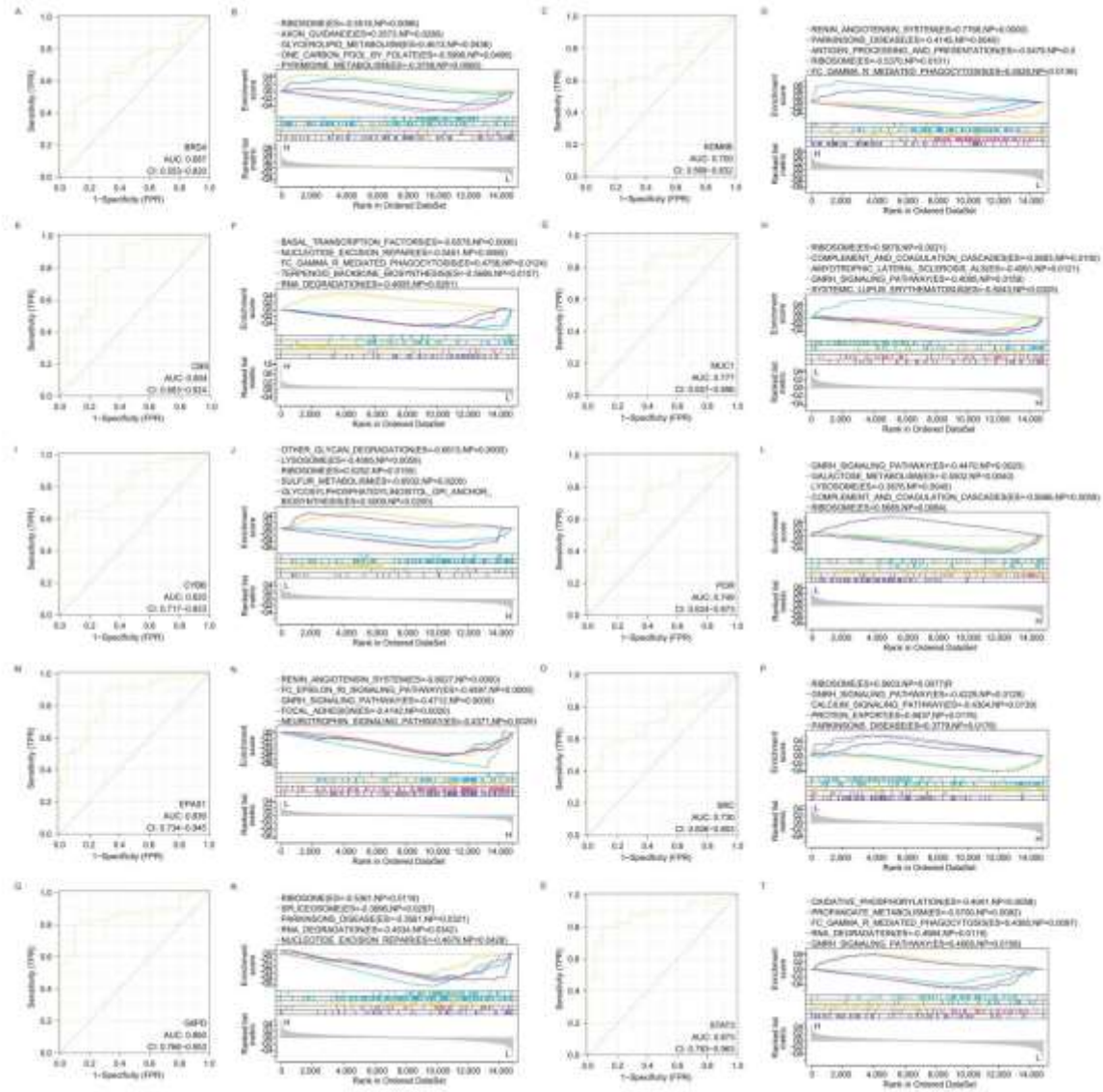
**Figure 7. ROC and GSEA analysis of hub genes**

(A-B) ROC and GSEA of BRD4. (C-D) ROC and GSEA of KDM6B. (E-F) ROC and GSEA of CBS. (G-H) ROC and GSEA of MUC1. (I-J) ROC and GSEA of CYBB. (K-L) ROC and GSEA of POR. (M-N) ROC and GSEA of EPAS1. (O-P) ROC and GSEA of SRC. (Q-R) ROC and GSEA of G6PD. (S-T) ROC and GSEA of STAT3.
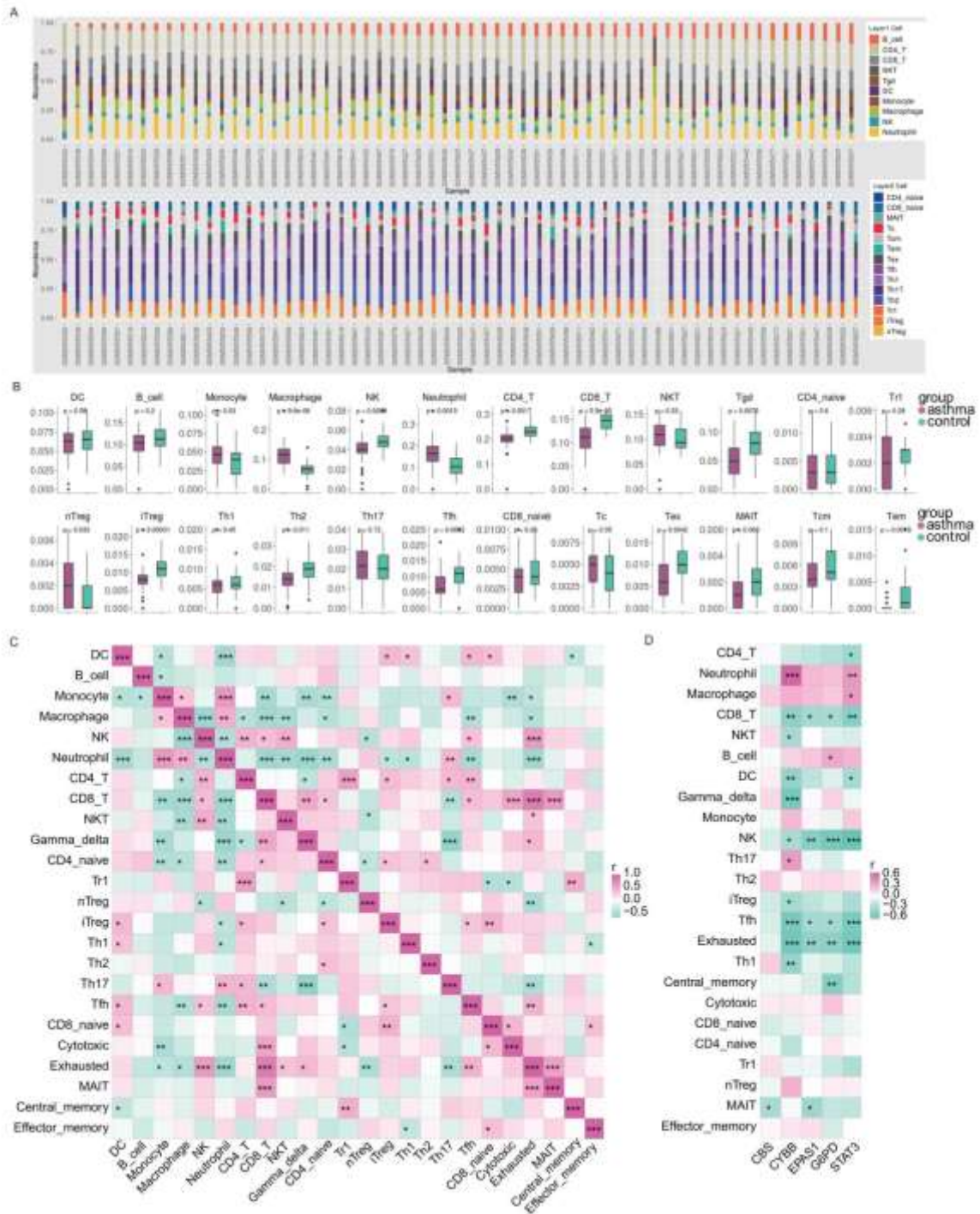
Figure 8. Immune cell composition landscape in asthma

(A) Stacked bar chart showing the proportions of various immune cell types in asthma

based on ImmuCellAI analysis. (B) Analysis of immune cell levels between asthma (red)

and control (green) samples. (C) Heatmap showing correlations between immune cell levels

in asthma samples. (D) Heatmap showing correlations between immune cell levels and hub genes in asthma samples.
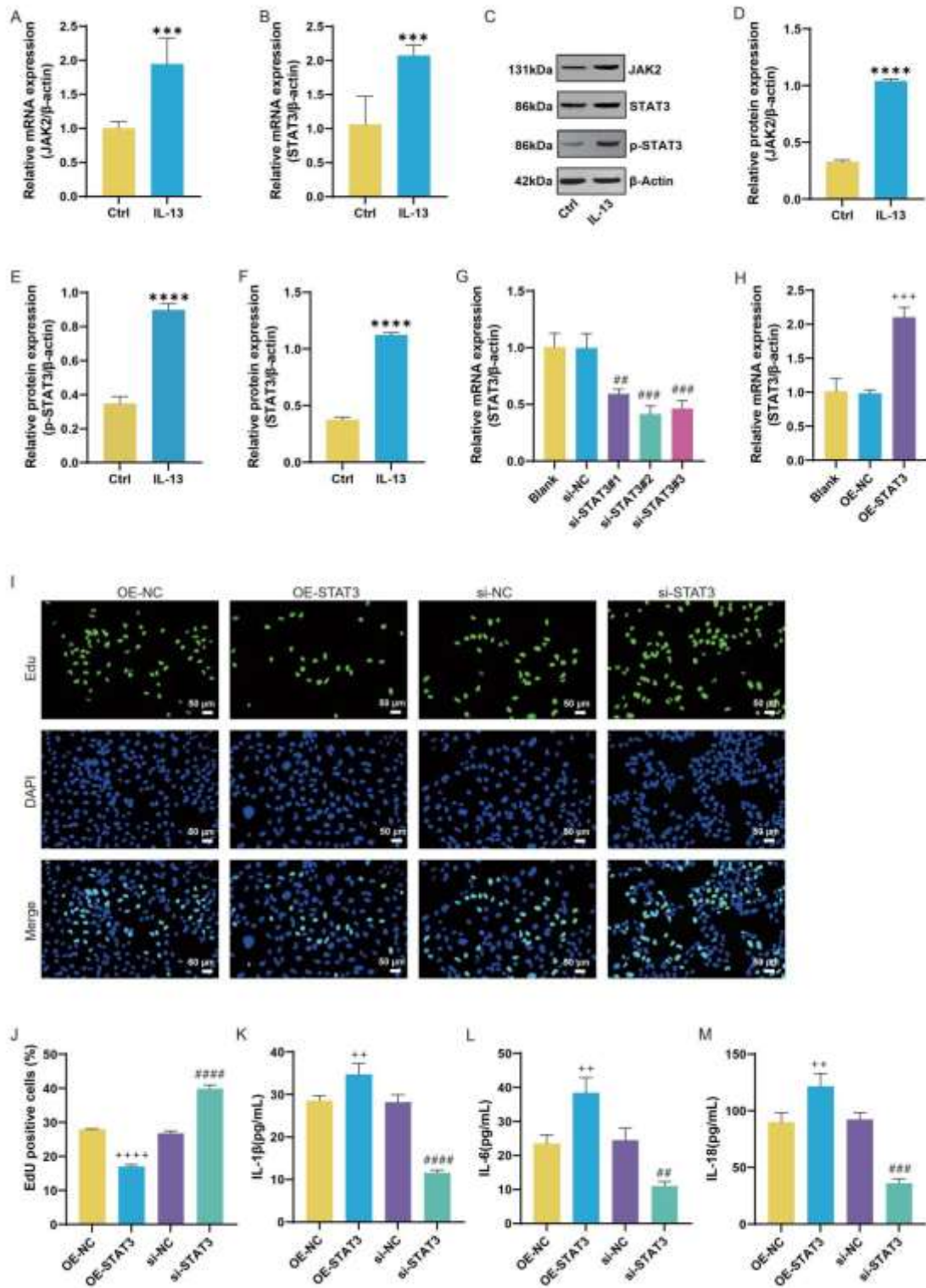
Figure 9. JAK2/STAT3 Involvement in IL-13 regulation of 16HBE cell proliferation and inflammation
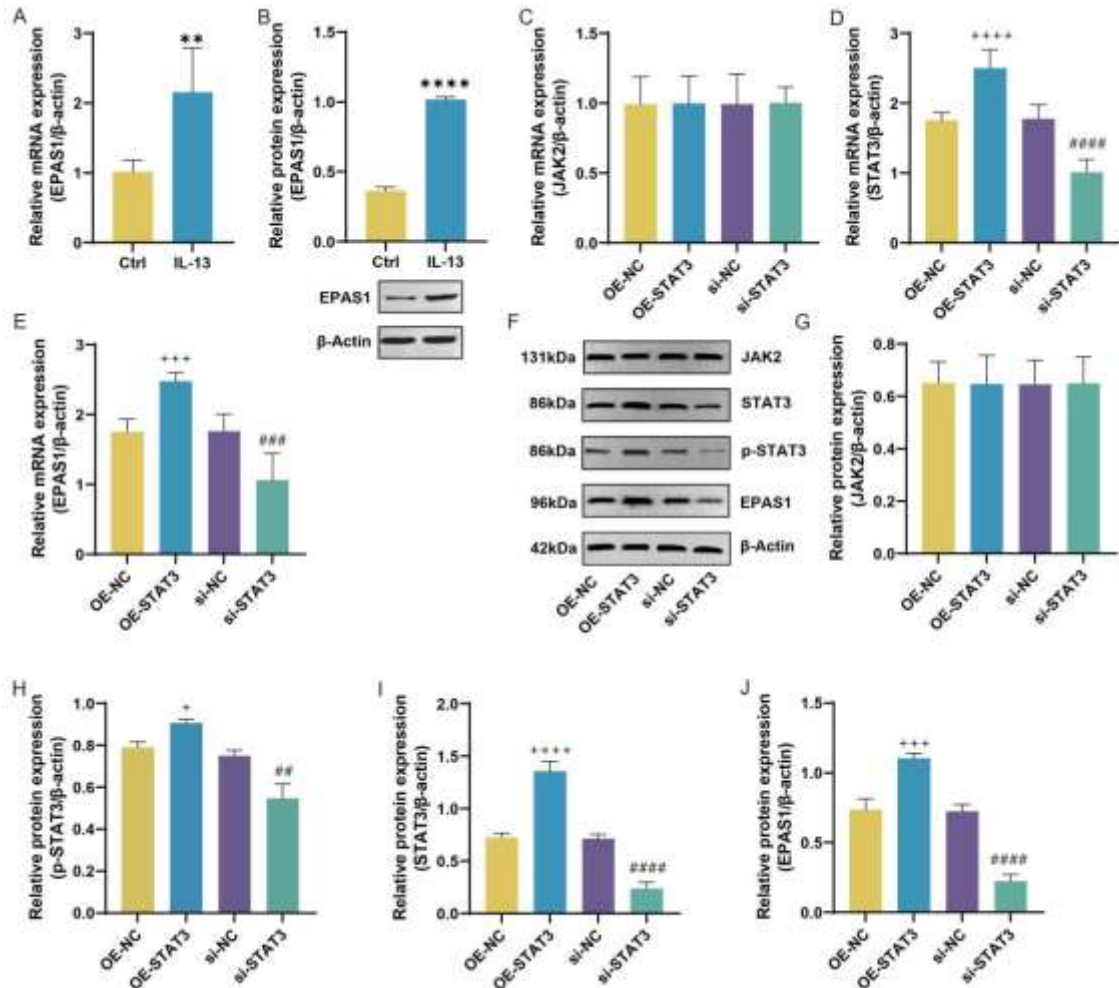
(A-B) QRT-PCR analysis of JAK2 and STAT3 mRNA levels in 16HBE cells from the Control (Ctrl) and IL-13 groups. (C-F) Western blot (WB) analysis of JAK2, phosphorylated STAT3 (p-STAT3), and STAT3 protein levels in 16HBE cells from the Ctrl and IL-13 groups. (G-H) qRT-PCR analysis of transfection efficiency for siRNA targeting STAT3 and overexpression plasmids. (I-J) Representative results and quantitative analysis of EDU staining in 16HBE cells from OE-NC, OE-STAT3, si-NC, and si-STAT3 groups. EDU-positive cells (green) are labeled, and cell nuclei are stained with DAPI (blue). (K-M) ELISA measurements of IL-1β (K), IL-6 (L), and IL-18 (M) in 16HBE cells from OE-NC, OE-STAT3, si-NC, and si-STAT3 groups. [***]$P<0.001$, [****]$P<0.0001$ compared to Ctrl group; [##]$P<0.01$, [###]$P<0.001$, [####]$P<0.0001$ compared to si-NC group; [++]$P<0.01$, [+++]$P<0.001$, [++++]$P<0.0001$ compared to OE-NC group.
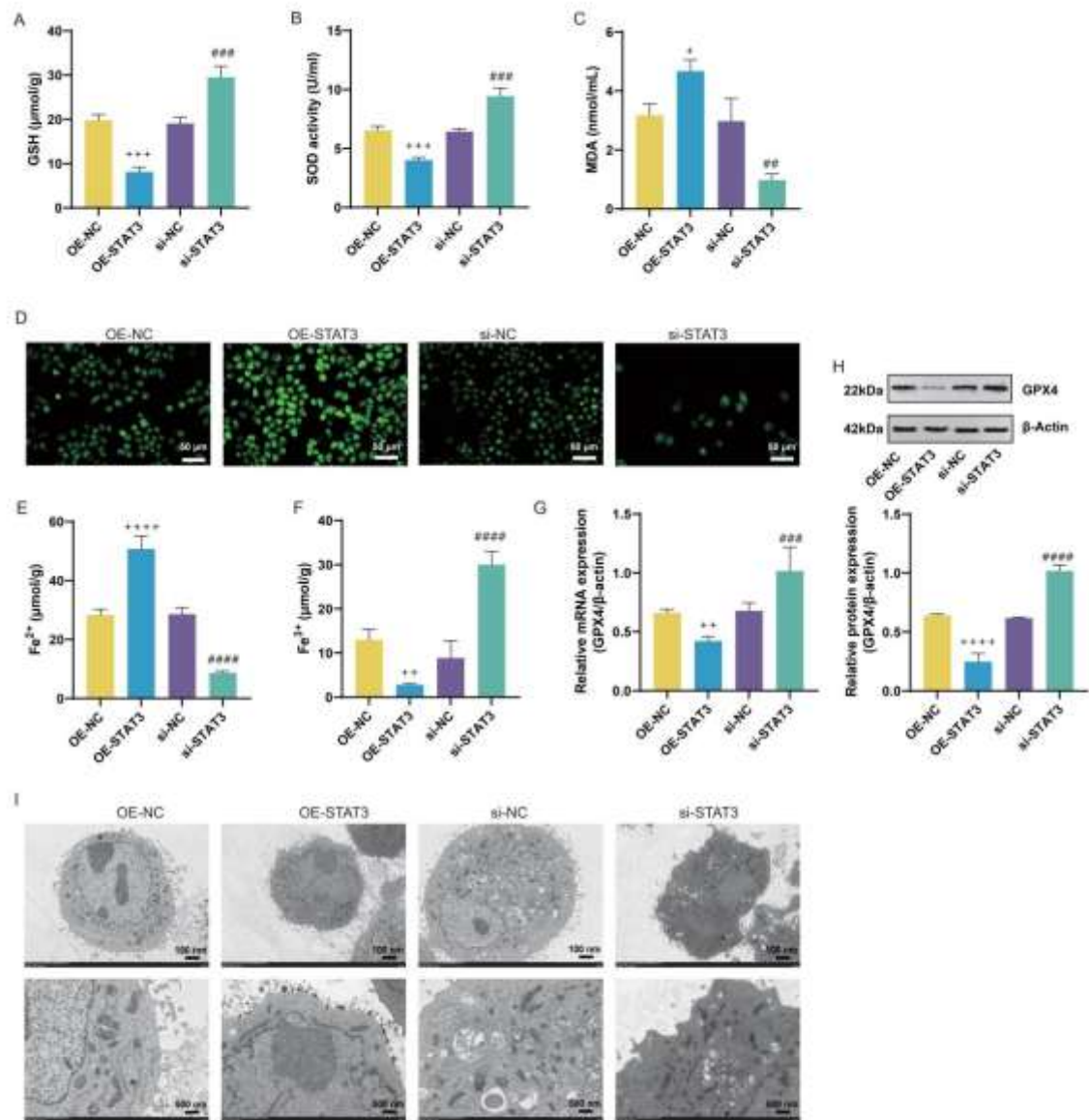
**Figure 10. IL-13 Induces ferroptosis in 16HBE cells via JAK2/STAT3**

(A-F) Measurement of GSH (A), SOD (B), MDA (C), ROS (D), Fe^{2+} (E), and Fe^{3+} (F)

levels in 16HBE cells from OE-NC, OE-STAT3, si-NC, and si-STAT3 groups using assay

kits. (G) QRT-PCR analysis of GPX4 mRNA levels in 16HBE cells from OE-NC, OE-

STAT3, si-NC, and si-STAT3 groups. (H) WB analysis of GPX4 protein levels in 16HBE

cells from OE-NC, OE-STAT3, si-NC, and si-STAT3 groups. (I) TEM analysis of

mitochondrial morphology in 16HBE cells from OE-NC, OE-STAT3, si-NC, and si-

STAT3 groups.$^{\#\#}P<0.01$, $^{\#\#\#}P<0.001$, $^{\#\#\#\#}P<0.0001$ compared to si-NC group. $^{+}P<0.05$,

$^{++}P<0.01$, $^{+++}P<0.001$, $^{++++}P<0.0001$ compared to OE-NC group.

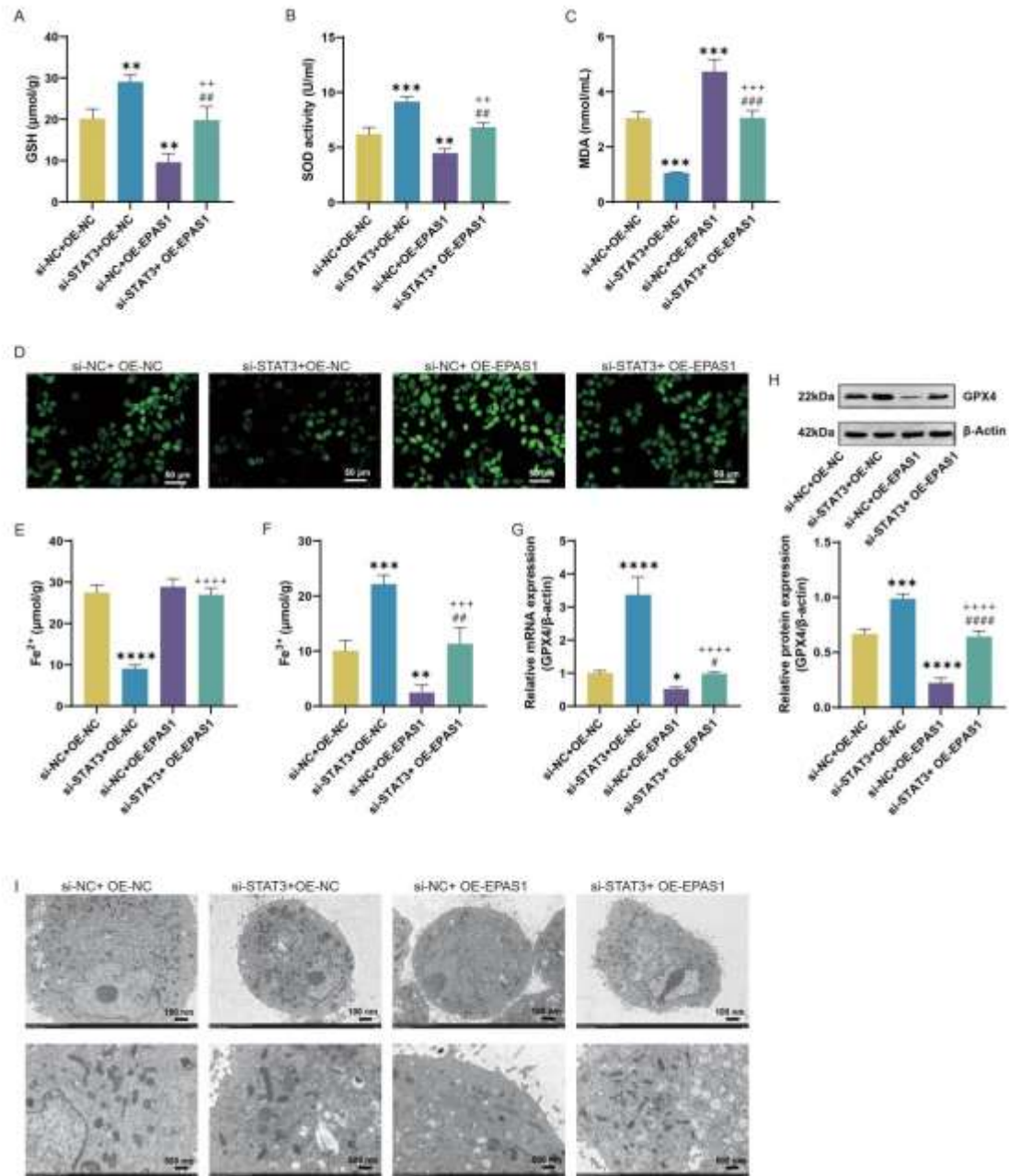**Figure 11. IL-13 upregulates EPAS1 via JAK2/STAT3**

(A) QRT-PCR analysis of EPAS1 mRNA levels in 16HBE cells from Ctrl and IL-13 groups. (C-E) QRT-PCR analysis of JAK2 (C), STAT3 (D), and EPAS1 (E) mRNA levels in 16HBE cells from OE-NC, OE-STAT3, si-NC, and si-STAT3 groups. (F-G) WB analysis of JAK2 (G), p-STAT3 (H), STAT3 (I), and EPAS1 (J) protein levels in 16HBE cells from OE-NC, OE-STAT3, si-NC, and si-STAT3 groups.$^{**}P<0.01$, $^{****}P<0.0001$ compared to Ctrl group. $^{\#\#}P<0.01$, $^{\#\#\#}P<0.001$, $^{\#\#\#\#}P<0.0001$ compared to si-NC group. $^{+}P<0.05$, $^{+++}P<0.001$, $^{++++}P<0.0001$ compared to OE-NC group.
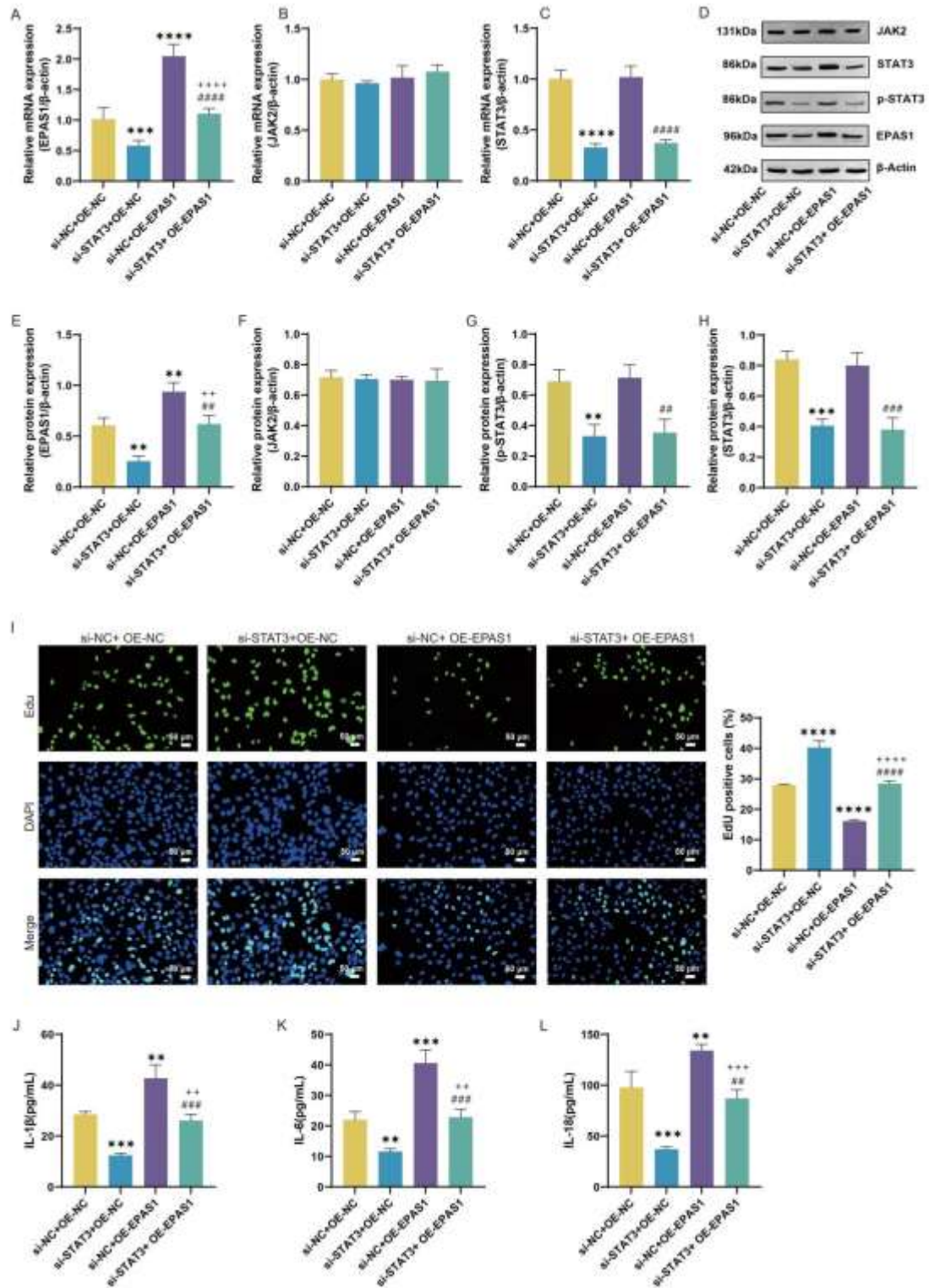
Figure 12. IL-13 regulates 16HBE cell proliferation and inflammation via JAK2/STAT3-mediated upregulation of EPAS1

(A-C) qRT-PCR analysis of EPAS1 (A), JAK2 (B), and STAT3 (C) mRNA levels in 16HBE cells from si-NC+OE-NC, si-STAT3+OE-NC, si-NC+OE-EPAS1, and si-STAT3+OE-EPAS1 groups. (D-H) WB analysis of EPAS1 (E), JAK2 (F), p-STAT3 (G), and STAT3 (H) protein levels in 16HBE cells from OE-NC, OE-STAT3, si-NC, and si-STAT3 groups. (I) Representative results and quantitative analysis of EDU staining in 16HBE cells from si-NC+OE-NC, si-STAT3+OE-NC, si-NC+OE-EPAS1, and si-STAT3+OE-EPAS1 groups. EDU-positive cells (green) are labeled, and cell nuclei are stained with DAPI (blue). (J-L) ELISA measurements of IL-1β (J), IL-6 (K), and IL-18 (L) in 16HBE cells from si-NC+OE-NC, si-STAT3+OE-NC, si-NC+OE-EPAS1, and si-STAT3+OE-EPAS1 groups. $^{**}P<0.01$, $^{***}P<0.001$, $^{****}P<0.0001$ compared to si-NC+OE-NC group. $^{+++}P<0.001$, $^{++++}P<0.0001$ compared to si-STAT3+OE-NC group. $^{\#\#}P<0.01$, $^{\#\#\#}P<0.001$, $^{\#\#\#\#}P<0.0001$ compared to si-NC+OE-EPAS1 group.

Figure 13. IL-13-induced ferroptosis in 16HBE cells regulated by EPAS1 upregulation via JAK2/STAT3

(A-C) Measurement of GSH (A), SOD (B), MDA (C), ROS (D), Fe^{2+} (E), and Fe^{3+} (F) levels in 16HBE cells from si-NC+OE-NC, si-STAT3+OE-NC, si-NC+OE-EPAS1, and si-STAT3+OE-EPAS1 groups using assay kits. (G) qRT-PCR analysis of GPX4 mRNA levels in 16HBE cells from si-NC+OE-NC, si-STAT3+OE-NC, si-NC+OE-EPAS1, and si-

STAT3+OE-EPAS1 groups. (H) WB analysis of GPX4 protein levels in 16HBE cells from si-NC+OE-NC, si-STAT3+OE-NC, si-NC+OE-EPAS1, and si-STAT3+OE-EPAS1 groups. (I) TEM analysis of mitochondrial morphology in 16HBE cells from si-NC+OE-NC, si-STAT3+OE-NC, si-NC+OE-EPAS1, and si-STAT3+OE-EPAS1 groups. [*]$P<0.05$, [**]$P<0.01$, [***]$P<0.001$, [****]$P<0.0001$ compared to si-NC+OE-NC group. [++]$P<0.01$, [+++]$P<0.001$, [++++]$P<0.0001$ compared to si-STAT3+OE-NC group. [#]$P<0.05$, [##]$P<0.01$, [###]$P<0.001$, [####]$P<0.0001$ compared to si-NC+OE-EPAS1 group.

SUPPLEMENTAL DATA

Table S1. Primers used for qRT-PCR

Gene	Forward primer(5'-3')	Reverse primer(5'-3')
JAK2	TGAGTTCGAAGCTAGCAGGGC	ACAGTTGTCTCCACCCTCTCC
STAT3	GGAGAAACAGGATGGCCCAA	ATCCAAGGGGCCAGAAACTG
EPAS1	ATGCTGTCTCTCTTGGCACC	GGTAAGAACCGACAGTGGCA
GPX4	AGTGAGGCAAGACCGAAGTA	GCTTCCCGAACTGGTTACAC
β-actin	CCCTGGAGAAGAGCTACGAG	GGAAGGAAGGCTGGAAGAGT

Table S2. Primary antibodies used for western blot

Gene	Manufacturer	Product Number	Theoretical Molecular Weight
P-STAT3	Affinity	AF3293	88kDa
STAT3	Affinity	AF6294	86kDa
JAK2	Affinity	AF6022	131KDa
EPAS1	Affinity	DG2928	96KDa
GPX4	Affinity	DF6701	22KDa
β-actin	Zs-BIO	TA-09	42kDa